Preparation of Hemp-Derived Activated Carbon Monoliths. Adsorption of Water Vapor

ARTICLE *in* INDUSTRIAL & ENGINEERING CHEMISTRY RESEARCH · JANUARY 2008

Impact Factor: 2.59 · DOI: 10.1021/ie070924w

Preparation of Hemp-Derived Activated Carbon Monoliths. Adsorption of Water Vapor

Juana M. Rosas, Jorge Bedia, José Rodríguez-Mirasol,* and Tomás Cordero

Chemical Engineering Department, School of Industrial Engineering, University of Málaga, Campus de El Ejido s/n, 29013 Málaga, Spain

Activated carbon monoliths have been obtained by the chemical activation of hemp canes with phosphoric acid. The effects of the carbonization temperature and the impregnation ratio on the porous structure and surface chemistry were studied. The porous structure of the activated carbon monoliths was characterized by N_2 adsorption−desorption and CO_2 adsorption isotherms. The surface chemistry of the carbons was analyzed by temperature-programmed desorption (TPD) and X-ray photoelectron spectroscopy (XPS), and the surface morphology was analyzed by scanning electron microscopy (SEM). Water vapor adsorption kinetics and capacities of the activated carbon monoliths were studied. The surface properties of the activated carbons were found to be strongly dependent on the carbonization temperature and the impregnation ratio. An activated carbon monolith with an apparent surface area of about 1500 m^2/g and a significant contribution of mesopores (mesopore volume of 0.6 cm^3/g) was obtained at 400 °C with an impregnation ratio of 2. The water vapor adsorption capacities were found to be comparable to that of silica gel, a material widely used as desiccant, because of the presence of residual phosphates and/or polyphosphates on the surface of the carbons.

Introduction

Hemp (*Cannabis sativa*) has been cultivated for centuries as a source of fiber for rope, sails, and clothing. The outer portion of the hemp stem contains strong and long fibers that provide the strength and quality attributed to the crop. The inner portion of the stem contains the cane, which is used for paper and building materials.

Hemp is currently being used for interesting applications in the textile, paper, and plastics industries, and the world production of hemp fiber was about 84000 tons in 2004. The hemp processing industry, however, generates a residue that represents 50−55% of the treated material.[1,2] The development of recycling processes of such biomass residues and research into new methods for obtaining high-value materials from hemp are generating great interest.

Activated carbon can be manufactured from many carbonaceous precursors such as wood, coal, coconut shells, lignin, and some polymers.[3−10] The world demand for activated carbon is steadily increasing because of its well-known extensive use as an adsorbent for purification and separation in many processes. The use of several agricultural byproducts, such as nutshells, fruit stones, sugarcane wastes, and sawdust from a few rapid growing wood species, as renewable precursors for low-cost activated carbon production is being widely studied.[11−21] Hemp and hemp byproducts might prove quite feasible for the production of activated carbon and present the advantage of the potential revalorization of a low-cost and easily processed material. In this respect, the preparation of activated carbon fibers by physical activation with steam and chemical activation with $ZnCl_2$ of hemp fibers has already been reported in the literature.[1,2]

The aim of this work was the preparation of activated carbon in monolith-like form by chemical activation of hemp canes with phosphoric acid and analysis of the influence of the activation temperature and the impregnation ratio on the activated carbon porous structure and surface chemistry.

* To whom correspondence should be addressed. Tel.: +34-952132886. Fax: +34-952132886. E-mail: mirasol@uma.es.

Experimental Section

Hemp stems were supplied by Alsativa (Sociedad Cooperativa Agraria Andaluza del Cáñamo, Pórtugos, Granada). After the fibers had been removed, the hemp canes that presented a monolithic structure with channels between 5 and 20 μm were used as the starting material for the preparation of activated carbon monoliths. The canes were cut into pieces that were about 3 cm long. The precursor was impregnated with 85% (w/w) H_3PO_4 aqueous solution at room temperature and dried for 24 h at 60 °C in a vacuum dryer. The values of the impregnation ratio, R (H_3PO_4/precursor mass ratio), used in this study were 1 and 2.

The impregnated hemp canes were activated under continuous N_2 flow (150 cm^3 STP/min) in a conventional tubular furnace. The activation temperature was reached at a heating rate of 10 °C/min and maintained for 2 h. Different activation temperatures within the range of 350−550 °C were studied. The activated samples were cooled inside the furnace under the same N_2 flow and then washed with distilled water at 60 °C until neutral pH and negative phosphate analysis in the eluate.[22] The resulting activated carbon monoliths were dried at 100 °C and weighed to determine the yield of the activation process (weight of activated carbon relative to raw material, on a dry basis). The activated carbon monoliths are denoted by the letter C followed by a number corresponding to the impregnation ratio and by a second number representing the activation temperature in degrees Celsius. Some carbon monoliths were obtained by carbonization of hemp canes under N_2 flow at different temperatures without impregnation of the activation agent. The carbon monoliths thus obtained are denoted by the letter C followed by the carbonization temperature in degrees Celsius.

The ultimate analysis of the samples was performed using a Leco CHNS-932 system, with the oxygen content calculated by difference. The ash content of the sample was calculated following the ASTM procedure.[23]

The porous structure of the activated carbon monoliths was evaluated by N_2 adsorption−desorption isotherms at −196 °C, performed with an Omnisorp 100cx apparatus (Coulter), and by CO_2 adsorption isotherms at 0 °C, carried out with an

10.1021/ie070924w CCC: $40.75
Published on Web 01/19/2008

Autosorb-1 apparatus (Quantachrome). Samples were previously outgassed for at least 8 h at 150 °C. From the N_2 isotherm, the apparent surface area (A_{BET}^{N2}) was determined by applying the BET equation.[24] The α_s method was used to obtain the values of the so-called external surface area (A_s^{N2}), that is, the surface area associated to the nonmicroporous structure; the micropore volume (V_s^{N2}); and the specific surface area (a_s^{N2}), using the high-resolution method proposed by Kaneko et al.,[25−27] with a nonporous carbon black sample (Elftex-120) as the standard.[28] The narrow mesopore volume was determined as the difference between the adsorbed volume of N_2 at a relative pressure of 0.95 and the micropore volume, V_s^{N2}.[25] This methodology covers only the mesopore range between 2 and 40 nm in size, according to the Kelvin equation.[28] From the CO_2 adsorption data, the narrow micropore volume (V_{DR}^{CO2}) and the apparent surface area (A_{DR}^{CO2}) were calculated using the Dubinin−Radushkevich equation.[29] The Horvath−Kawazoe[30] method applied to the N_2 adsorption data was used to obtain the pore size distributions.

The surface chemistry of the samples was analyzed by temperature-programmed desorption (TPD) and X-ray photoelectron spectroscopy (XPS). TPD profiles were obtained in a custom quartz fixed-bed reactor placed inside an electrical furnace. The samples were heated from room temperature to 900 °C at a heating rate of 10 °C/min in helium flow (200 cm^3 STP/min). The amounts of CO and CO_2 evolved from the samples were monitored with nondispersive infrared (NDIR) gas analyzers (Siemens ULTRAMAT 22). XPS analyses of the samples were performed using a 5700C model Physical Electronics spectrometer with Mg Kα radiation (1253.6 eV). For the analysis of the XPS peaks, the C 1s peak position was set at 284.5 eV and used as a reference to locate the other peaks.[31−33] The fitting of the XPS peaks was done by the least-squares method using Gaussian−Lorentzian peak shapes. The surface texture of the samples was characterized by scanning electron microscopy (SEM). Scanning electron micrographs were obtained using a JEOL JSM-840 instrument, working at a high voltage of 20−25 kV.

Water vapor adsorption−desorption analysis was performed in a gravimetric thermobalance system (CI Electronics). The thermobalance automatically measures the weight of the sample as a function of time. Water adsorption isotherms were obtained by setting pressure intervals relative to the saturation vapor pressure (P/P_o) at 20 °C. Before the experiments, samples were outgassed under vacuum (10^{-3} Torr) in a drying vacuum oven at 110 °C for at least 24 h to eliminate water physisorbed on the carbon surface.

Results and Discussion

Table 1 summarizes the analytical and structural characteristics of the precursor used for the preparation of activated carbon monoliths. Hemp canes show a small apparent surface area as measured with N_2. However, the values of surface area and micropore volume measured with CO_2 indicate the presence of slightly narrow microporosity in this material. The ash content of the raw material is relatively low.

The effects of two main variables on the activation process with regard to the surface chemistry and the development of the porous structure were examined; specifically, we considered the impregnation ratio and the activation temperature. Table 2 reports the yields and ultimate analyses of the resulting carbons and activated carbon monoliths. The yields for the carbons were significantly lower than those for the activated carbons at the same treatment temperature. The activation agent restricts the formation of tars during the carbonization process, thus increasing the yield of the remaining solid product.[3] Yields of about 40% were obtained for the activated carbon monoliths, similar to the values obtained using other biomass natural wastes[4,5,15] and hemp fibers prepared by a different activation process.[1,2] The yields decrease as activation temperature and impregnation ratio increase, as a consequence of a higher dehydration of the carbonaceous structure of the precursor. The carbon content decreases with temperature, but it increases with the impregnation ratio. Higher impregnation ratios restrict the formation of tars and volatiles and produce a deeper dehydration, thus increasing the carbon content, as previously observed by Williams et al.[2] The amount of oxygen increases with the activation temperature as a result of the incorporation into the carbon matrix formed of the oxygen bound to the phosphorus.[4,5] It decreases with the impregnation ratio, probably because of the effectiveness of the washing process, which is greater at high impregnation ratios as a consequence of the wider porous structure obtained (as discussed below).

Table 1. Analytical and Structural Characteristics of the Hemp Canes Used for Activated Carbon Preparation

ash content (% db)	0.8
ultimate analysis (% dab)	
C	49.7
H	5.4
N	0.4
O	44.5
major components	
cellulose	40
hemicellulose	20
lignin	20
apparent surface area (m^2/g)	
A_{BET}^{N2}	9
A_{DR}^{CO2}	102
micropore volume (cm^3/g)	
V_s^{N2}	–
V_{DR}^{CO2}	0.039

Table 2. Yields and Ultimate Analyses of Hemp-Derived Carbon and Activated Carbon Monoliths

	yield (% db)	C (% daf)	H (% daf)	N (% daf)	O (% daf)
C-450	21.1	90.2	3.0	0.7	6.1
C-550	20.2	95.6	2.1	0.6	1.7
C-800	16.6	98.1	0.5	0.6	0.8
C1-450	47.1	68.2	2.6	0.2	29.0
C2-350	51.2	84.0	3.3	0.3	12.6
C2-400	43.6	80.6	1.9	0.2	17.3
C2-450	40.4	78.6	2.2	0.3	18.9
C2-500	37.9	74.8	2.4	0.3	22.5
C2-550	34.4	73.3	2.0	0.3	24.4

Porous Structure. Figure 1 shows the N_2 adsorption−desorption isotherms at −196 °C for carbon and activated carbon monoliths obtained from hemp cane at different carbonization or activation temperatures and impregnation ratios.

The isotherms of the carbon monoliths are of type I and exhibit an almost horizontal plateau starting at very low relative pressure, indicating that the porous structure consists predominantly of very narrow micropores. As carbonization temperature increases, there is an increase of the micropore volume, as revealed by the increase in N_2 adsorbed at low relative pressures. The carbon monolith obtained at 800 °C shows a small hysteresis loop at relative pressures of about 0.5, which indicates the slight development of narrow mesopores at this carbonization temperature.

Significantly higher N_2 adsorption volumes were found for the activated carbon monoliths than for the carbon monoliths prepared at the same temperatures. This result clearly shows the effect of the phosphoric acid activation in the porosity

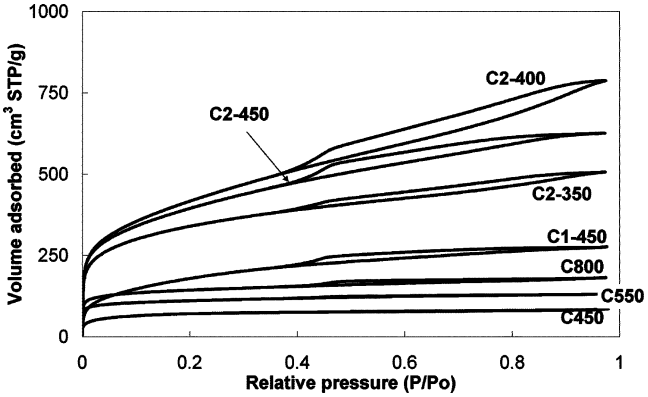

Figure 1. N_2 adsorption−desorption isotherms of hemp-derived carbon and activated carbon monoliths.

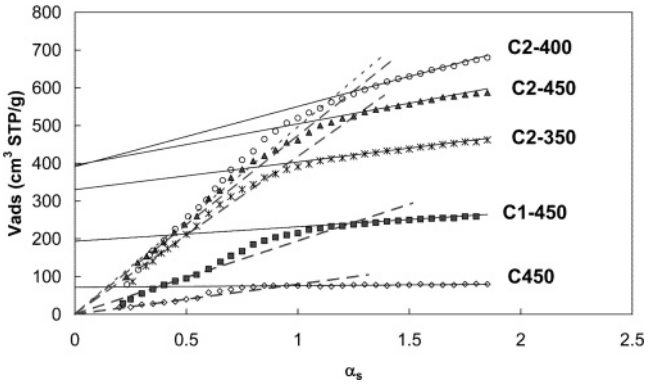

Figure 2. α_s curves of carbon and activated carbon monoliths.

development of hemp canes. All of the activated carbon monoliths show a modified type I isotherm, corresponding to a well-developed microporous structure with a significant contribution of mesoporosity, which depends on both the impregnation ratio and the activation temperature. The total N_2 adsorbed volume, which provides a first approximation of porosity development, increases with increasing activation temperature up to 400 °C and then decreases significantly at higher temperatures.

An increase in the relative amount of activation agent results in a higher development of porosity. The shape of the isotherms, with a more rounded knee and a larger hysteresis loop at high relative pressures, reveals that an increase in the impregnation ratio gives rise to a considerable widening of the porous structure of the resulting carbon, with a significantly higher contribution of mesoporosity.

Figure 2 presents the α_s plots of the carbon obtained at 450 °C and some activated carbon monoliths. These plots show the amount of N_2 adsorbed versus α_s, the ratio of the amount adsorbed by a nonporous standard (Elftex-120) at each relative pressure to that adsorbed at $P/P_o = 0.4$.[34] The linear region for α_s values greater than 1.2 (linear multilayer region, solid lines) corresponds to adsorption on the nonmicroporous surface of the solid. Back-extrapolation of that linear branch provides the value of the total micropore volume (after the volume of N_2 gas adsorbed is converted to a liquid volume). The slope of this linear region of the α_s plots provides the external or nonmicroporous surface area of the activated carbons. Kaneko et al.[25−27] proposed that, for data obtained using the α_s method, the specific surface area of a sample, a_s, can be determined from the slope of the straight line that fits α_s values <1 and goes through the origin (dotted line). The plots at different temperatures show that all of the activated carbon monoliths have a significant contribution of microporosity. The micropore volume

Table 3. Structural Characteristics of Carbon and Activated Carbon Monoliths

	N_2 isotherm					CO_2 isotherm	
	A_{BET}^{N2} (m^2/g)	a_s^{N2} (m^2/g)	V_s^{N2} (cm^3/g)	A_s^{N2} (m^2/g)	V_{mes}^{N2} (cm^3/g)	A_{DR}^{CO2} (m^2/g)	V_{DR}^{CO2} (cm^3/g)
C-450	256	249	0.112	12	0.020	484	0.184
C-550	397	403	0.180	19	0.024	481	0.183
C-800	516	499	0.233	36	0.050	578	0.220
C1-450	695	504	0.296	117	0.115	313	0.119
C2-350	1214	1199	0.517	205	0.239	817	0.311
C2-400	1574	1415	0.623	439	0.609	621	0.236
C2-450	1481	1370	0.625	303	0.344	670	0.255
C2-500	1250	1070	0.475	384	0.535	713	0.271
C2-550	1209	1112	0.469	330	0.469	742	0.282

increases with activation temperature up to 400 °C. An increase of the activation temperature to 450 °C did not produce an increase of the microporous structure, as indicated by the back-extrapolation of the multilayer region. Increasing the impregnation ratio produced a higher micropore volume and external surface area.

The structural characteristics of the carbon and activated carbon monoliths are reported in Table 3. This table summarizes the apparent surface areas obtained using the BET and α_s methods, the micropore volumes and external surface areas obtained using the α_s method, and the mesopore volumes derived from the N_2 adsorption data. In addition, the apparent surface areas and micropore volumes obtained by the application of the DR method to the CO_2 isotherms are also included in Table 3. The apparent surface areas obtained by the BET and α_s methods are very similar. The differences between the micropore volumes obtained with N_2 and CO_2 isotherms confirm a wider microporosity than for the monolithic carbons.[7] N_2 adsorption is carried out throughout the entire range of relative pressures, so that can cooperative filling of wider micropores occurs, whereas CO_2 adsorption at relative pressures <0.03 allows primary filling of only narrow micropores.

Phosphoric acid is combined with organic species to form phosphate and polyphosphate bridges that connect and cross-link biopolymer fragments. The insertion of phosphate groups separates the organic species, driving a process of expansion that, after removal of the acid, leaves the matrix in an expanded state with an accessible pore structure and is thus responsible for the development of porosity.[3,11,15−17] Chemical activation of hemp cane with phosphoric acid proceeds at relatively low temperatures of 300−400 °C, giving rise to a considerable development of micro- and mesoporosity. At higher temperatures, these phosphate and polyphosphate bridges become thermally unstable, causing shrinkage of the porous carbon structure.

An increase of the impregnation ratio results in the development of porosity, mostly of larger pores. This development appears to occur as more activating agent is incorporated into the carbonaceous matrix of the precursor. The addition of phosphoric acid causes the higher insertion of phosphate esters, which results in the greater expansion of the structure with increasing impregnation ratio.[3,16] At an activation temperature of 400 °C and an impregnation ratio of 2, activated carbon in the form of monolith with an apparent surface area of more than 1500 m^2/g and an external area of 450 m^2/g was obtained.

Figure 3 shows the micropore size distributions of carbon C-450 and different activated carbon monoliths. Carbon C-450 has a poorly developed microporous structure. Most of the micropores of the activated carbon monoliths have an effective pore width in the range of 7−9 Å. At low activation temperature, 350 °C, the distributions show a significant contribution of

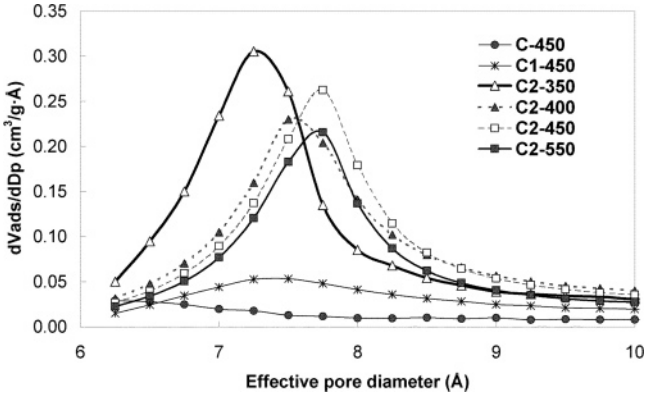

Figure 3. Micropore size distributions of carbon and activated carbon monoliths.

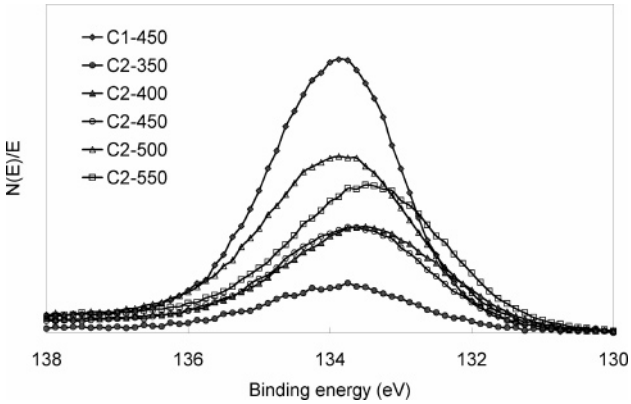

Figure 4. XPS P 2p spectra of activated carbon monoliths.

narrow micropores, with a maximum at about 7 Å. At higher activation temperature, wider micropores are produced. The micropore size distribution of the activated carbon monolith obtained at 550 °C shows the effect of the contraction of the microporous structure. An increase of the impregnation ratio results not only in the development of the microporosity but also in an increase of the micropore size.

Surface Chemistry. To study the surface chemistry of the samples, temperature-programmed desorption (TPD) and X-ray photoelectron spectroscopy (XPS) analysis were performed. In addition, the morphology of the surfaces was analyzed by scanning electron microscopy (SEM).

The surface element distributions of the canes, cane ashes, and carbon and activated carbon monoliths were studied by XPS. Quantitative analysis of the peaks was performed to obtain the mass surface concentrations; the results are summarized in Table 4. The cane ashes show very significant amounts of phosphorus, calcium, and magnesium, most probably in the form of carbonates. The main elements found on the surfaces of the activated carbon monoliths are carbon and oxygen, with lower amounts of phosphorus, which is retained in the structure during the activation procedure. Other elements such us nitrogen and silicon were also detected, but at very low concentrations.

An increase of the activation temperature led to the incorporation of a higher amount of phosphorus into the structure of the activated carbons, either combined with the organic structure, in the form of phosphates, or physically entrapped.[3] Only a slight decrease seems to occur for the highest activation temperature studied. An increase of the impregnation ratio resulted in a decrease in the amount of phosphorus remaining in the carbon matrix after the washing process. Thus, carbon C1-450 shows the highest amount of phosphorus despite having the lowest impregnation ratio. This is probably due to the narrow microporous structure presented by this monolithic activated carbon, with a very low mesopore contribution. Phosphorus compounds seem to be bonded to the carbon matrix in a stronger form in this microporous structure,[3] which reduces the extraction efficiency during the washing process. An alternative explanation for the high P content in these materials is a lower efficiency in the washing step. These samples contain narrow micropores, and the washing solution could have difficulty penetrating these pores and removing soluble P compounds.

The XPS P 2p spectra of different activated carbon monoliths are shown in Figure 4. The P 2p spectrum of phosphorus shows a band with a main peak at a binding energy of about 133.7 eV, which is characteristic of pentavalent tetracoordinated phosphorus (PO_4) as in polyphosphates and/or phosphates.[3,5,35−37] An increase of the activation temperature from 350 to 500 °C shifted the binding energy of the main peak to a value close to 134.0 eV, which Wu and Radovic[38] assigned to $C-O-PO_3$ groups. A further increase of the activation temperature to 550 °C moved the peak to a binding energy of 133.4 eV, which is characteristic of a P atom bonded to one C atom and three O atoms, as in $C-PO_3$ groups.[38]

Phosphoric acid appears to activate hemp cane through the formation of phosphate and polyphosphate bridges that cross-link biopolymer fragments, avoiding the contraction of the structure by pyrolysis. Part of the activating agent is removed during the washing step, leading to a carbon matrix in an expanded state with an accessible pore structure.[39] However, part of the P remains on the carbon surface after the washing step. The XPS P 2p results seem to indicate the presence of $C-O-PO_3$ and $C-PO_3$ groups on the surface of the monolithic activated carbons. The contribution of the $C-O-PO_3$ groups on the carbon surface increases up to an activation temperature of 500 °C, but then decreases at higher temperature. The presence of small amount of phosphorus as P_2O_5 cannot be ruled out (BE = 135.6 eV).[37]

TPD analysis was used to characterize the different oxygen surface groups of the activated carbons, whose nature and amount depend on the starting material and the activation treatment.[40] Carbon−oxygen groups of acidic character (carboxylic, lactonic) evolve as CO_2 upon thermal desorption, whereas the nonacidic (carbonyl, ether, quinone) and phenol groups give rise to CO. Anhydride surface groups evolve as both CO and CO_2.[33]

Table 4. Mass Surface Concentrations (%) Determined by XPS Quantitative Analysis of Different Hemp-Derived Samples

	C 1s	O 1s	N 1s	P 2p	Ca 2p	S 2p	Mg 2s	K 2p	Si 2p	Na 1s
cane ash	9.70	48.28	–	9.50	20.49	1.75	8.98	0.66	–	0.62
cane	65.65	30.79	0.93	1.12	0.97	–	–	–	0.49	0.05
C-800	87.63	8.87	0.25	0.81	2.17	–	–	–	0.27	–
C1-450	61.95	26.90	–	11.14	–	–	–	–	–	–
C2-350	79.51	16.72	0.83	2.21	–	–	–	–	0.72	–
C2-400	82.25	11.90	–	4.69	–	–	–	–	1.16	–
C2-450	78.33	16.64	–	4.63	–	–	–	–	0.41	–
C2-500	75.26	16.49	0.36	7.57	–	–	–	–	0.32	–
C2-550	78.14	14.41	0.23	6.41	–	–	–	–	0.82	–

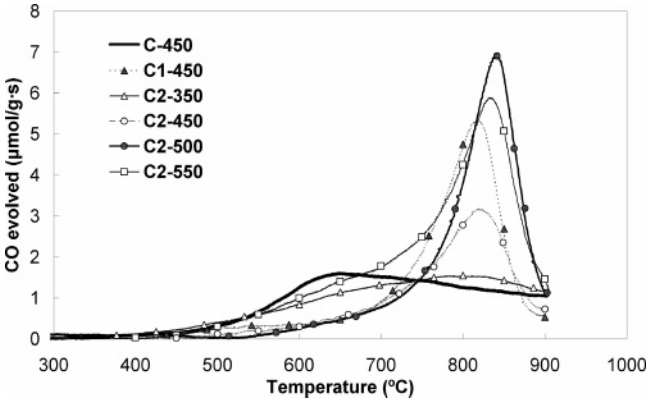

Figure 5. CO evolution during the TPD of carbon and activated carbon monoliths.

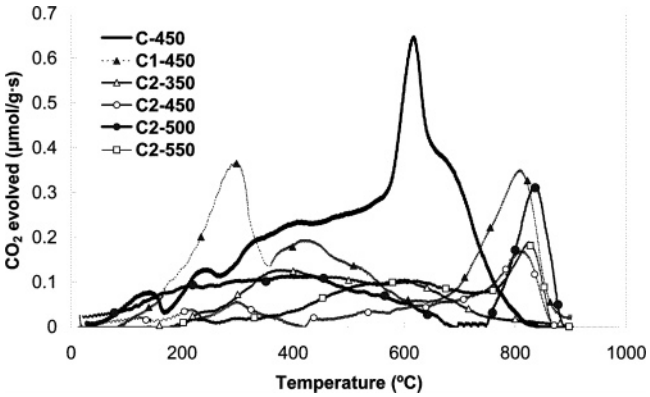

Figure 6. CO_2 evolution during the TPD of carbon and activated carbon monoliths.

Figures 5 and 6 show the results of CO and CO_2 TPD, respectively, for different carbon and activated carbon monoliths. The activation process results in the thermal stabilization of the oxygen surface groups that evolve as CO. The main band for the evolution of CO for carbon C-450 appears at ~650 °C. However, the most significant CO evolution for the activated carbon monoliths takes place at higher temperatures (800−850 °C), and this change in the thermal stability of the oxygen surface groups that evolve as CO seems to be significant for activation temperatures above 350 °C. Wu and Radovic[38] found the same release of CO groups at high temperatures for P-containing carbons and associated this behavior with the presence of relatively weak $C-O-PO_3$ groups on the carbon surface at high temperatures. Therefore, for the activated carbon monoliths, most of the CO evolved at high temperatures, and a lower amount desorbed at temperatures below 700 °C in the form of anhydride, phenol, and ether groups. When the activation temperature is increased to 550 °C, the formation of $C-PO_3$ groups probably from $C-O-PO_3$ groups seems to take place, and CO is evolved from anhydride, phenol, and ether surface groups during TPD at lower temperatures. Puziy et al.[4,5] and Fu et al.[35] found that an increase of the treatment temperature results in greater amounts of phenol and ether groups.

CO_2 desorbed in lower amounts than CO, indicating a lower presence of carboxyl, lactonic, and anhydride groups. Carbon C-450 displays a marked peak located at ~625 °C that might be related to the decomposition of carbonate groups. The bulk alkali metal carbonates (sodium, calcium, and potassium) melt before decomposing at temperatures above 820 °C. However, examples of the decomposition of alkaline metal carbonates occurring at temperatures below the melting point during the heating of carbonate−carbon mixtures have been reported in the literature.[14,41−43] The high stability of the CO_2 groups that evolve at temperatures above 800 °C, probably as a result of secondary reactions,[44,45] is noteworthy. Diffusion of the evolved gases is rather slow in narrow micropores and a free CO might react to CO_2 with surface-bound oxygen.

Table 5. CO and CO_2 Evolved from TPD Analyses

	CO (mmol/g)	CO_2 (mmol/g)
C-450	3.21	0.93
C1-450	3.96	0.66
C2-350	3.11	0.30
C2-400	3.68	0.43
C2-450	4.08	0.27
C2-500	4.73	0.44
C2-550	5.81	0.29

A second TPD experiment was performed on activated carbon C1-450 immediately after the first one. The results obtained showed a small but constant presence of CO at higher temperatures (850 °C), with a very small peak of CO_2. The presence of $C-O-PO_3$ groups can explain these results. It is possible that the oxygen bonded to C and P evolves as CO at higher temperatures in the first TPD run. The "free" CO generates active surface sites that are susceptible to attack probably from the P atom and the hydroxyl group linked to phosphorus, thus producing $C-PO_2-O-C$. During the second TPD run at high temperature, this new group might again result in the desorption of CO. The CO_2 evolution can be attributed to the previously discussed secondary reactions.

Table 5 reports the amounts of CO and CO_2 evolved during the TPD experiments for the carbon and activated carbon monoliths. The amount of CO evolved increases with the activation temperature, but no significant variation was found with increasing impregnation ratio. As previously mentioned, a small amount of CO_2 desorbed from the activated carbon monoliths, with this amount being higher for hemp cane carbonized at 450 °C.

SEM micrographs of activated carbons from canes of hemp are presented in Figure 7a and b. The cross section of monolithic activated carbon C1-450 is shown in Figure 7a; the external diameter is about 7 mm, and the internal diameter is 3 mm. In the case of the carbons, a decrease in the external and internal diameters of the monoliths in relation to those of the original cane occurred, and this reduction was more pronounced at higher carbonization temperatures ($\Phi_e \approx 5$ mm for C-450 and $\Phi_e \approx 4$ mm for C-800). This process can be of great interest for the revalorization of hemp residues through the production of activated carbon monoliths with a highly developed porous structure. Figure 7b shows activated carbon monolith C2-450 at higher magnification, where the heterogeneous porous distribution along the cane due to the characteristics of the cane itself can be seen.

Figure 8 shows photographs of (a) hemp cane, (b) carbon monolith C-800, and activated carbon monolith C2-400. This figure clearly shows the contraction of the monolith structure submitted to carbonization at 800 °C and the expansion of the activated carbon diameter, compared to those of the hemp cane.

Water Vapor Adsorption. Figure 9 shows the water vapor adsorption isotherms obtained in a thermogravimetric system at 20 °C for monolithic carbons C-800, C1-450, and C2-450. The isotherm of the traditional desiccant silica gel is also included in the figure for comparison. The carbon monolith displays the typical carbon water vapor isotherm (type V isotherm) with very low uptake at low relative pressures, much lower than that of silica gel. However, both activated carbons, C1-450 and C2-450, exhibit water vapor adsorption capacities

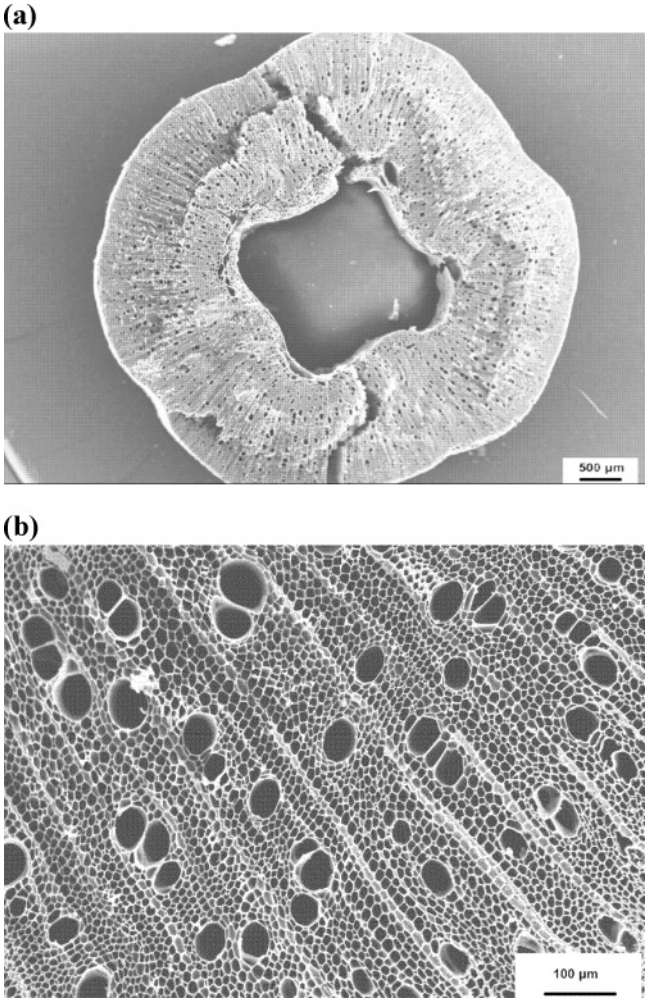

Figure 7. SEM micrographs of (a) C1-450 (cross section), (b) C2-450.

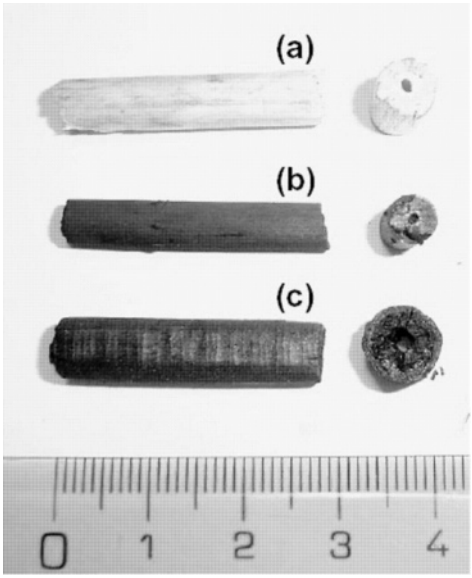

Figure 8. Digital photographs of (a) hemp cane, (b) C-800 monolithic carbon, (c) C2-400 activated carbon monolith.

at low relative pressures ($P/P_o < 0.5$) that are comparable to that of the silica gel and significantly higher capacities at high relative pressures ($P/P_o > 0.5$). It has been shown that the presence of inorganic matter at the carbon surface enhances the water vapor adsorption capacity[46] and this enhancement is even more pronounced in the presence of phosphorus.[47,48] Both

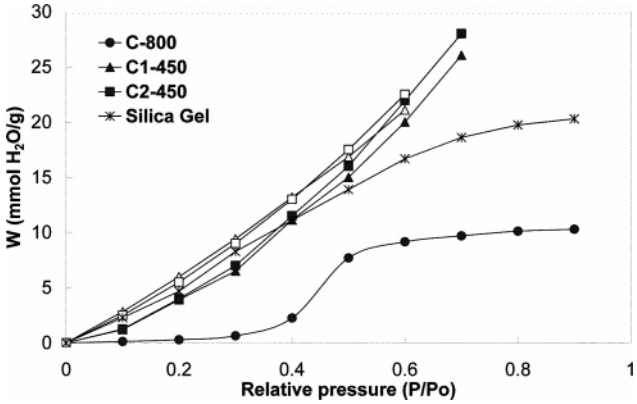

Figure 9. Water vapor adsorption−desorption isotherms at 20 °C for C-800, C1-450, C2-450, and silica gel (adsorption, solid symbols; desorption, open symbols).

carbons have significant amounts of phosphorus dispersed on their surfaces. The XPS analyses suggest that the phosphorus is found as polyphosphate or phosphate esters, with significant amounts of oxygen that can act as active sites for water vapor adsorption.

It is interesting to note that carbon C1-450 exhibits an adsorption−desorption isotherm similar to that of C2-450, despite the more developed porous structure of the latter. This is probably due to the higher amount of phosphorus on C1-450, as revealed by the XPS analyses (see Table 4).

Water adsorption isotherms are very different in their shapes from the corresponding isotherms for organic vapors and other inorganic gases. Water−water attractive forces are much stronger than water−carbon surface forces, resulting in behavior that is opposite to that observed for the typical adsorption of organic vapors and inorganic gases on carbons. Contrary to the pore-filling mechanism of different organic vapors, where adsorption takes place via the formation of successive layers prior to capillary condensation, the water adsorption process begins with the adsorption of water molecules on the surface active centers.[49,50] These molecules act as new active centers for the formation of water clusters. When these clusters have sufficient dispersive force, they enter the micropores, and micropore filling occurs.[50−52] In our case, the oxygen bound to phosphorus dispersed on the carbon surfaces acts as surface active centers, increasing the water vapor capacities throughout the relative pressure range.

The appearance of a hysteresis loop is a characteristic phenomenon of water vapor adsorption−desorption on activated carbons, as a consequence of the different pore-filling and -emptying mechanisms.[40] Carbons with a wide pore size distribution show a marked adsorption hysteresis, because water molecules adsorb in the form of larger water clusters, which next enter the micropore volume and desorb through uniform molecular evaporation.

The adsorption of water vapor on the carbon surface is a very complex process that involves the diffusion of water molecules and water clusters in slit-shaped micropores whose width is less than the free path of the gas molecules at atmospheric pressure. Harding et al.[53] analyzed the existence of diffusion barriers in the kinetics of water adsorption−desorption on activated carbons. Other works[54,55] have studied the kinetics of adsorption as a function of water vapor relative pressure, in terms of rate constants.

Figure 10 depicts the water vapor adsorption kinetics at 20 °C and different relative pressures for carbon C1-450, where M_t is the amount of water adsorbed at time t and M_e is the

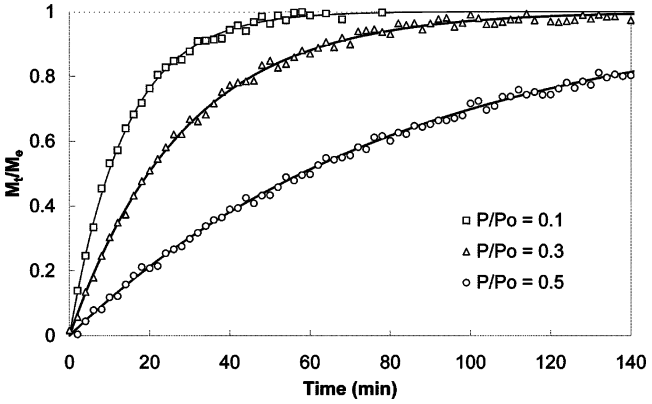

Figure 10. Water vapor adsorption kinetics at 20 °C and different relative pressures for C1-450 (open symbols, experimental data; solid lines, fitting to LDF model).

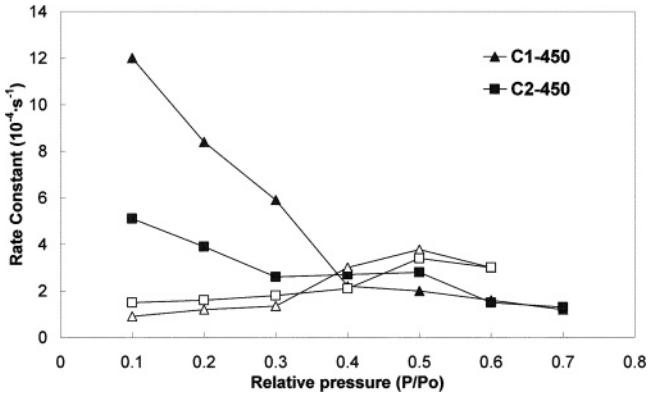

Figure 11. Water vapor adsorption−desorption kinetics at 20 °C for C1-450 and C2-450 (adsorption, solid symbols; desorption, open symbols).

equilibrium amount of absorbed water. These data can be properly fitted to a linear-driving-force (LDF) mass-transfer model[53−55]

$$\frac{M_t}{M_e} = 1 - e^{-kt}$$

where k is the rate constant. Under isobaric conditions, a plot of $\ln(1 - M_t/M_e)$ versus time gives a straight line with a slope of $-k$. The solid lines in Figure 10 represent the fitting of the experimental data to the LDF model. This LDF kinetic model was used to calculate the adsorption−desorption rate constants for the different carbons. A similar behavior was found for C2-450.

Figure 11 shows the variation of the rate constant k as a function of relative pressure for carbons C1-450 and C2-450. For the adsorption (solid symbols), two regions can be observed. The first, at low relative pressures, is related to the adsorption of the water molecules on the active centers and presents the highest values of the rate constant. The second region located at medium to high relative pressures, which has the lowest rate constants, represents the growth of water clusters around the previously chemisorbed molecules through the formation of hydrogen bonds. This behavior agrees fairly well with the results reported in the literature.[53−55] At low relative pressures, adsorption takes places preferentially at the adsorption centers and occurs at a relatively high rate. As adsorption proceeds at increasing relative pressure, the degree of covering increases, thus decreasing the number of free adsorption sites and increasing the diffusion limitation of water vapor molecules moving through the partially filled micropores after adsorption on the primary centers, which seems to reduce the rate of adsorption. At high relative pressures, the adsorption sites are occupied by water clusters grown around the previously chemisorbed molecules on primary sites, and the adsorption process, less rapid, is associated with the filling of micropores and the condensation of water on meso- and macropores. C1-450 shows higher adsorption rate constants at low relative pressures ($P/P_o < 0.4$) than C2-450, probably because of the higher amounts of oxygen and phosphorus on this carbon that hasten the adsorption process.

The rate constant for water vapor desorption as a function of relative pressure is also plotted in Figure 11. The lowest rates for the desorption process were obtained in the low relative pressure range. This could be due to the more difficult removal of the water molecules that are strongly bonded to the active centers during the final stage of desorption.

These results should be relevant for desiccant applications, such as sorption cooling/heating systems, where low-cost porous solids that exhibit relatively significant water vapor adsorption at low relative pressures (type I moderate isotherms) are preferred.

Conclusions

Natural hemp canes have been used to prepare activated carbon monoliths. The preparation of these activated carbon monoliths by chemical activation with phosphoric acid resulted in significant pore development with a high contribution from mesopores, giving materials that are very suitable for catalyst reactions, liquid-phase adsorption processes, and many other applications. Activated carbon monoliths with an apparent surface area of 1500 m^2/g and a mesopore volume of 0.6 cm^3/g were obtained.

The pore development is strongly dependent on the activation temperature and impregnation ratio. Monolithic activated carbons present a maximum in the apparent surface area and external area at an activation temperature of 400 °C. At higher activation temperatures, the breakdown of the phosphate ester bridges appears to cause the contraction of the porous structure, thus reducing the apparent surface area and micropore volume.

An increase of the impregnation ratio results in high pore development. As more phosphoric acid is incorporated into the precursor structure, the expansion process increases, causing greater development of porosity, mostly mesopores.

An increase of the activation temperature increases the amount of phosphorus retained on the carbon matrix, as polyphosphates or phosphates esters. The presence of phosphorus on the activated carbon monoliths increases the water vapor adsorption capacity, probably because of oxygen atoms bound to the phosphorus, which act as active sites for the water vapor adsorption.

Acknowledgment

The authors thank the Ministry of Science and Education of Spain for financial support (DGICYT, Projects CTQ2006/11322 and PPQ2003-07160). J.B. acknowledges the assistance of the Ministry of Science and Education of Science and Education of Spain for the award of an FPI grant.

Nomenclature

A_{BET}^{N2} = apparent surface area obtained by the BET method (m^2/g)
A_{DR}^{CO2} = apparent area of narrow micropores (m^2/g)
a_s^{N2} = specific area obtained by the α_s method (m^2/g)

A_s^{N2} = external area obtained by the α_s method (m^2/g)
ASTM = American Society for Testing and Materials
BE = binding energy (eV)
BET = Brunauer, Emmett, and Teller
D_p = effective pore diameter (Å)
DR = Dubinin−Radushkevich
FTIR = Fourier transform infrared
k = rate constant (s^{-1})
LDF = linear driving force
M_e = amount of water adsorbed at equilibrium (mmol/g)
M_t= amount of water adsorbed at time t (mmol/g)
NDIR = nondispersive infrared
P/P_o = relative vapor pressure
R = impregnation ratio (H_3PO_4 mass/carbon precursor mass)
SEM = scanning electron microscopy
STP = standard temperature−pressure conditions
T = temperature (°C)
TPD = temperature-programmed desorption
V_{ads} = volume of nitrogen adsorbed (cm^3/g)
V_{DR}^{CO2} = micropore volume obtained by the DR method (cm^3/g)
V_{mes}^{N2} = mesopore volume (cm^3/g)
V_s^{N2} = micropore volume obtained by the α_s method (cm^3/g)
W = amount of water adsorbed (mmol/g)
XPS = X-ray photoelectron spectroscopy

Greek Letters

α_s = normalized adsorption = V_{ads} at any relative pressure/V_{ads} at a relative pressure of 0.4 for a nonporous standard solid, in this case, Elftex 120a
Φ_e = external diameter (mm)

Literature Cited

(1) Williams, P. T.; Reed, A. R. Pre-formed Activated Carbon Matting Derived from the Pyrolysis of Biomass Natural Fiber Textile Waste. *J. Anal. Appl. Pyrolysis* **2003**, *70*, 563.

(2) Williams, P. T.; Reed, A. R. High Grade Activated Carbon Matting Derived from the Chemical Activation and Pyrolysis of Natural Fibre Textile Waste. *J. Anal. Appl. Pyrolysis* **2004**, *71*, 971.

(3) Jagtoyen, M.; Derbyshire, F. Activated Carbons from Yellow Poplar and White Oak by H_3PO_4 Activation. *Carbon* **1998**, *36*, 1085.

(4) Puziy, A. M.; Poddubnaya, O. I.; Martínez-Alonso, A.; Suárez-García, F.; Tascón, J. M. D. Synthetic Carbons Activated with Phosphoric Acid. I. Surface Chemistry and Ion Binding Properties. *Carbon* **2002**, *40*, 1493.

(5) Puziy, A. M.; Poddubnaya, O. I.; Martínez-Alonso, A.; Suárez-García, F.; Tascón, J. M. D. Surface Chemistry of Phosphorous-Containing Carbons of Lignocellulosic Origin. *Carbon* **2005**, *43*, 2857.

(6) Hsu, L.; Teng, H. Influence of Different Chemical Reagents on the Preparation of Activated Carbons from Bituminous Coal. *Fuel Process. Technol.* **2000**, *64*, 155.

(7) Rodríguez-Mirasol, J.; Cordero, T.; Rodríguez, J. J. Activated Carbons from CO_2 Partial Gasification of Eucalyptus Kraft Lignin. *Energy Fuels* **1993**, *7*, 133.

(8) Rodríguez-Mirasol, J.; Cordero, T.; Rodríguez, J. J. High-Temperature Carbons from Kraft Lignin. *Carbon* **1996**, *1*, 43.

(9) Rodríguez-Mirasol, J.; Cordero, T.; Rodríguez, J. J. Preparation and Characterization of Activated Carbons from Eucalyptus Kraft Lignin. *Carbon* **1993**, *1*, 87.

(10) González-Serrano, E.; Cordero, T.; Rodríguez-Mirasol, J.; Rodríguez, J. J. Development of Porosity upon Chemical Activation of Kraft Lignin with $ZnCl_2$. *Ind. Eng. Chem. Res.* **1997**, *36*, 4832.

(11) Blanco Castro, J.; Bonelli, P. R.; Cerilla, E. G.; Cukierman, A. L. Phosphoric Acid Activation of Agricultural Residues and Bagasse from Sugar Cane: Influence of the Experimental Conditions on Adsorption Characteristics of Activated Carbons. *Ind. Eng. Chem. Res.* **2000**, *39*, 4166.

(12) Tancredi, N.; Cordero, T.; Rodríguez-Mirasol, J.; Rodríguez, J. J. Activated Carbons from Uruguayan Eucalyptus Wood. *Fuel* **1996**, *15*, 1701.

(13) Marquez-Montesinos, F.; Cordero, T.; Rodríguez-Mirasol, J.; Rodríguez, J. J. CO_2 and Steam Gasification of a Grapefruit Skin Char. *Fuel* **2002**, *81*, 423.

(14) Molina-Sabio, M.; Rodríguez-Reinoso, F.; Catarla, F.; Sellés, M. J. Porosity in Granular Carbons Activated with Phosphoric Acid. *Carbon* **1995**, *33*, 1105.

(15) Vernersson, T.; Bonelli, P. R.; Cerrella, E. G.; Cukierman, A. L. *Arundo donax* Cane as a Precursor for Activated Carbons Preparation by Phosphoric Acid Activation. *Bioresour. Technol.* **2002**, *83*, 95.

(16) Solum, M. S.; Pugmire, R. J.; Jagtoyen, M.; Derbyshire, F. Evolution of Carbon Structure in Chemically Activated Wood. *Carbon* **1995**, *33*, 1247.

(17) Molina-Sabio, M.; Rodríguez-Reinoso, F. Role of Chemical Activation in the Development of Carbon Porosity. *Colloids Surf. A: Physicochem. Eng. Aspects* **2004**, *241*, 15.

(18) El-Sheikh, A. H.; Newman, A. P.; Al-Daffaee, H. K.; Phull, S.; Cresswell, N. Characterization of Activated Carbons Prepared from a Single Cultivar of Jordanian Olive Stones by Chemical and Physicochemical Techniques. *J. Anal. Appl. Pyrolysis* **2004**, *71*, 151.

(19) Gergova, K.; Eser, S. Effects of the Activation Method on the Pore Structure of Activated Carbons from Apricot Stones. *Carbon* **1996**, *34*, 879.

(20) Toles, C. A.; Marshall, W. E.; Wartelle, L. H.; Johns, M. M. Acid Activated Carbons from Almond Shells: Physical, Chemical and Adsorptive Properties and Estimated Cost of Production. *Bioresour. Technol.* **2000**, *71*, 87.

(21) Toles, C. A.; Marshall, W. E.; Wartelle, L. H.; McAloon, A. Steam or Carbon Dioxide Activated Carbons from Almond Shells: Physical, Chemical and Adsorptive Properties and Estimated Cost of Production. *Bioresour. Technol.* **2000**, *75*, 197.

(22) González-Serrano, E.; Cordero, T.; Rodríguez-Mirasol, J.; Cotoruelo, L.; Rodríguez, J. J. Removal of Water Pollutants with Activated Carbons Prepared from H_3PO_4 Activation of Lignin from Kraft Black Liquors. *Water Res.* **2004**, *38*, 3043.

(23) *Standard Test Method for Total Ash Content of Activated Carbon*; ASTM: West Conshohocken, PA, 2004; Standard D2866-94.

(24) Brunauer, S.; Emmett, P. H.; Teller, E. Adsorption of Gases in Multimolecular Layers. *J. Am. Chem. Soc.* **1938**, *60*, 309.

(25) Kaneko, K.; Ishii, C. Superhigh Area Determination of Microporous Solids. *Colloids Surf.* **1992**, *67*, 203.

(26) Kaneko, K.; Ishii, C.; Ruike, M.; Kuwabara, H. Origin of Superhigh Surface Area and Microcrystalline Graphitic Structures of Activated Carbons. *Carbon* **1992**, *30*, 1075.

(27) Kaneko, K. Determination of Pore Size and Pore Size Distribution. I. Adsorbents and Catalysts. *J. Membr. Sci.* **1994**, *96*, 59.

(28) Gregg, S. I.; Sing, K. S. W. *Adsorption, Surface Area and Porosity*; Academic Press: London, 1982.

(29) Dubinin, M. M.; Zaverina, E. D.; Radushkevich, L. V. Sorption and Structure of Active Carbons. I. Adsorption of Organic Vapors. *J. Phys. Chem. (USSR)* **1947**, *21*, 1351.

(30) Horvath, G.; Kawazoe, K. Method for the Calculation of Effective Pore Size Distribution in Molecular Sieve Carbon. *J. Chem. Eng. Jpn.* **1983**, *16*, 470.

(31) Biniak, S.; Szymanski, G.; Siedlewski, J.; Swiatkowski, A. The Characterization of Activated Carbons with Oxygen and Nitrogen Surface Groups. *Carbon* **1997**, *35*, 1799.

(32) Desimoni, E.; Casella, G. I.; Morone, A.; Salvi, A. M. XPS Determination of Oxygen Containing Functional Groups on Carbon-Fibre Surfaces and the Cleaning of These Surfaces. *Surf. Interface Anal.* **1990**, *15*, 627.

(33) Figuereido, J. L.; Pereira, M. F. R.; Freitas, M. M. A.; Órfão, J. J. M. Modification of the Surface Chemistry of Activated Carbons. *Carbon* **1999**, *37*, 1379.

(34) Carrott, P. J. M.; Roberts, R. A.; Sing, K. S. W. Adsorption of Nitrogen by Porous and Non-Porous Carbons. *Carbon* **1987**, *25*, 59.

(35) Fu, R.; Liu, L.; Huang, W.; Sun, P. Studies on the Structure of Activated Carbon Fibers Activated by Phosphoric Acid. *J. Appl. Polym. Sci.* **2002**, *87*, 2253.

(36) Moulder, J. F.; Stickle, W. F.; Sobol, P. E.; Bomben, K. D. *Handbook of X-ray Photoelectron Spectroscopy*; Chastain, J., King, R. C., Jr., Eds.; Physical Electronics, Inc.: Eden Prairie, MN, 1995; pp 4872−4875.

(37) Puziy, A. M.; Poddubnaya, O. I.; Ziatdinov, A. M. On the Chemical Structure of Phosphorus Compounds in Phosphoric Acid-Activated Carbon. *Appl. Surf. Sci.* **2006**, *252*, 8036.

(38) Wu, X.; Radovic, L. R. Inhibition of Catalytic Oxidation of Carbon/Carbon Composites by Phosphorus. *Carbon* **2006**, *44*, 141.

(39) Suárez-García, F.; Martínez-Alonso, A.; Tascón, J. M. D. Activated Carbon Fibers from Nomex by Chemical Activation with Phosphoric Acid. *Carbon* **2004**, *42*, 1419.

(40) Bansal, R. C.; Donnet, J. B.; Stoeckli, F. *Active Carbon*; Marcel Dekker: New York, 1988; Chapter 2.

(41) Kapteijn, F.; Abbel, G.; Moulijn, J. A. Carbon Dioxide Gasification of Carbon Catalyzed by Alkali Metals. Reactivity and Mechanism. *Fuel* **1984**, *63*, 1036.

(42) Lillo-Ródenas, M. A.; Cazorla-Amorós, D.; Linares-Solano, A. Understanding Chemical Reactions between Carbons and NaOH and KOH. An Insight in to the Chemical Activation Mechanism. *Carbon* **2003**, *41*, 267.

(43) Nevskaia, D. M.; Santianes, A.; Muñoz, V.; Guerrero-Ruíz, A. Interaction of Aqueous Solutions of Phenol with Commercial Activated Carbon: An Adsorption and Kinetic Study. *Carbon* **1999**, *37*, 1065.

(44) Hall, P. J.; Calo, J. M. Secondary Interactions upon Thermal Desorption of Surface Oxides from Coal Chars. *Energy Fuels* **1989**, *3*, 370.

(45) Boehm, H. P. Surface Oxides on Carbon and Their Analysis: A Critical Assessment. *Carbon* **2002**, *40*, 145.

(46) Bedia, J.; Rodríguez-Mirasol, J.; Cordero, T. Water Vapor Adsorption on Lignin-Based Activated Carbons. *J. Chem. Technol. Biotechnol*. **2007**, *82*, 548.

(47) Bedia, J.; Rodríguez-Mirasol, J.; Cordero, T. Influence of Nitrogen and Phosphorous in the Water Vapour Adsorption. Presented at Carbon 2004, Providence, RI, July 11−16, 2004; Paper 46.4 (A041).

(48) Bedia, J.; Rodríguez-Mirasol, J.; Cordero, T. Estudio de la Adsorción de Vapor de Agua a Diferentes Temperaturas sobre Carbones Activos y Silica Gel. In *VIII Reunión del Grupo Español del Carbón: Baeza, del 6 al 9 de noviembre de 2005*; Paper C18, 181.

(49) Daou, K.; Wang, R. Z.; Xia, Z. Z. Desiccant Cooling Air Conditioning: A Review. *Renewable Sustainable Energy Rev.* **2006**, *10*, 55.

(50) Mahajan, O. P.; Youssef, A.; Walker, P. L., Jr. Surface-Modified Carbons for the Drying of Gas Streams. *Sep. Sci. Technol*. **1982**, *17*, 1019.

(51) Brennan, J. K.; Bandosz, T. J.; Thomson, K. T.; Gubbins, K. E. Water in Porous Carbons. *Colloids Surf. A* **2001**, *187*−*188*, 539.

(52) McCallum, C. L.; Bandosz, T. J.; McGrother, C.; Müller, E. A.; Gubbins, K. E. A Molecular Model for Adsorption of Water on Activated Carbon: Comparison of Simulation and Experiment. *Langmuir* **1999**, *15*, 533.

(53) Harding, A. W.; Foley, N. J.; Norman, P. R.; Francis, D. C.; Thomas, K. M. Diffusion Barriers in the Kinetics of Water Vapor Adsorption/Desorption on Activated Carbons. *Langmuir* **1998**, *14*, 3858.

(54) Cossarutto, L.; Zimny, T.; Kaczmarczyk, J.; Siemieniewska, T.; Bimer, J.; Weber, J. V. Transport and Sorption of Water Vapor in Activated Carbons. *Carbon* **2001**, *39*, 2339.

(55) Foley, N. J.; Thomas, K. M.; Forshaw, P. L.; Stanton, D.; Norman, P. R. Kinetics of Water Vapor Adsorption on Activated Carbon. *Langmuir* **1997**, *13*, 2083.

Received for review July 6, 2007
Revised manuscript received November 8, 2007
Accepted November 8, 2007

IE070924W